

Genesis, evolution, and apocalypse of Loop Current rings

F. Andrade-Canto,^{1, a)} D. Karrasch,^{2, b)} and F. J. Beron-Vera^{3, c)}

¹⁾*Instituto de Investigaciones Oceanológicas, Universidad Autónoma de Baja California, Ensenada, Baja California, México*

²⁾*Technische Universität München, Zentrum Mathematik, Garching bei München, Germany*

³⁾*Department of Atmospheric Sciences, Rosenstiel School of Marine and Atmospheric Science, University of Miami, Miami, Florida, USA*

(Dated: 2 January 2022)

We carry out assessments of the life cycle of Loop Current vortices, so-called rings, in the Gulf of Mexico by applying three objective (i.e., observer-independent) coherent Lagrangian vortex detection methods on velocities derived from satellite altimetry measurements of sea-surface height (SSH). The methods reveal material vortices with boundaries that withstand stretching or diffusion, or whose fluid elements rotate evenly. This involved a technology advance that enables framing vortex genesis and apocalypse robustly and with precision. We find that the stretching- and diffusion-withstanding assessments produce consistent results, which show large discrepancies with Eulerian assessments that identify vortices with regions instantaneously filled with streamlines of the SSH field. The even-rotation assessment, which is vorticity-based, is found to be quite unstable, suggesting life expectancies much shorter than those produced by all other assessments.

PACS numbers: 02.50.Ga; 47.27.De; 92.10.Fj

I. INTRODUCTION

The Loop Current System, namely, the Loop Current itself and the anticyclonic (counterclockwise) mesoscale (100–200-km radius) vortices, so-called rings, shed from it, strongly influences the circulation, thermodynamics, and biogeochemistry of the Gulf of Mexico (GoM).³⁴ As important long-range carriers, westward-propagating Loop Current rings (LCRs) provide a potential mechanism for the remote connectivity between the GoM's western basin and the Caribbean Sea.^{1,3,6,7,21,24,25} In particular, bringing warm Caribbean Sea water within, the heat content of the LCRs is believed to be as significant as for LCRs to promote the intensification of tropical cyclones (hurricanes).³² On the other hand, as regions of strong flow shear, LCRs may be capable of producing structural damage on offshore oil drilling rigs.¹⁸ For all these reasons, LCRs are routinely monitored.³³

LCRs leave footprints in satellite altimetric sea-surface height (SSH) maps,²³ so sharp that the routine detection of LCRs consists in the identification of regions filled with closed streamlines of the SSH field assuming a geostrophic balance, a practice widely followed in oceanography.⁵ However, this eddy detection approach uses instantaneous Eulerian information to reach long-term conclusions about fluid (i.e., Lagrangian) transport, which are invariably surrounded by uncertainty due to the unsteady nature of the underlying flow. At the heart of the issue with Eulerian eddy diagnostics of this type is their dependence on the observer viewpoint:²⁹ they give

different results for observers that rotate and translate relative to one another. The issue is most easily grasped by bringing up, one more time as we believe is central yet widely overlooked, the example first discussed by Haller⁹ and thereafter by others.^{4,10,13,15} Consider the exact solution to the Navier–Stokes equation in two spatial dimensions: $v(x, t) = (x^1 \sin 4t + x^2(2 + \cos 4t), x^1(\cos 4t - 2) - x^2 \sin 4t)$, where $x = (x^1, x^2) \in \mathbb{R}^2$ denotes position and $t \in \mathbb{R}$ is time. The flow streamlines are closed at all times suggesting an elliptic structure (i.e., a vortex). However, this flow actually hides a rotating saddle (pure deformation), as it follows by making $(x^1, x^2) \mapsto (\bar{x}^1, \bar{x}^2) = (x^1 \cos 2t - x^2 \sin 2t, x^1 \sin 2t + x^2 \cos 2t)$, under which $v(x, t) \mapsto (\bar{x}^2, \bar{x}^1) \equiv \bar{v}(\bar{x})$. In other words, the de-facto oceanographic eddy detection diagnostic⁵ misclassifies the flow as vortex-like. The \bar{x} -frame is special inasmuch the flow in this frame is steady, and thus flow streamlines and fluid trajectories coincide. Hence short-term exposition pictures of the velocity field by the observer in the \bar{x} -frame determine the long-term fate of fluid particles. The only additional observation to have in mind to fully determine the Lagrangian motion is that the observer in the \bar{x} -frame rotates (at angular speed 2). This tells us that the flow under consideration is not actually unsteady as there is a frame (\bar{x}) in which it is steady. In a truly unsteady flow there is no such distinguished observer for whom the flow is steady.²⁶ Thus one can never be sure which observer gives the right answer when the de-facto oceanographic eddy detection diagnostic^{5,23} is applied. As a consequence, neither false positives nor false negatives can be ruled out,⁴ and thus the significance of life expectancy estimates is unclear.

Our goal here is to carry out objective (i.e., observer-independent) assessments of the life cycle of LCRs. This will be done in line with recent but growing work that makes systematic use of geometric tools from nonlinear

^{a)}Electronic mail: andcanfer@gmail.com

^{b)}Electronic mail: karrasch@ma.tum.de

^{c)}Electronic mail: fberon@miami.edu

dynamics to frame vortices objectively.^{2,4,8,10–17,19,31} We will specifically apply three methods which define *coherent Lagrangian vortex* boundaries as material loops that (i) defy stretching,^{13,14} (ii) resist diffusion,¹⁶ and (iii) whose elements rotate evenly,¹⁵ respectively. The fluid enclosed by such loops can be transported for long distances without noticeable dispersion.^{36,37}

The rest of the paper is organized as follows. In the next section we briefly review the formal definition of each of the above coherent Lagrangian vortex notions. In Sec. III we present a technology that enables framing vortex genesis and apocalypse robustly and with precision. Section IV presents the data (satellite altimetry) on which our assessments of the life cycle of LCRs are applied. It also presents numerical details of the implementation of the vortex detection methods, and introduces the databases which deliver Eulerian assessments of the “birth” and “decease” dates of LCRs, which are used for reference. The results of our study are presented in Section V. Finally, concluding remarks are offered in Section VI.

II. COHERENT LAGRANGIAN RING DETECTION

Consider

$$F_{t_0}^t : x_0 \mapsto x(t; x_0, t_0), \quad (1)$$

$$\eta_\lambda^\pm(x_0) := \sqrt{\frac{\lambda_2(x_0) - \lambda^2}{\lambda_2(x_0) - \lambda_1(x_0)}} \xi_1(x_0) \pm \sqrt{\frac{\lambda^2 - \lambda_1(x_0)}{\lambda_2(x_0) - \lambda_1(x_0)}} \xi_2(x_0), \quad (2)$$

where $\lambda_1(x_0) < \lambda^2 < \lambda_2(x_0)$. Here, $\{\lambda_i(x_0)\}$ and $\{\xi_i(x_0)\}$ satisfying

$$0 < \lambda_1(x_0) \equiv \frac{1}{\lambda_2(x_0)} < 1, \quad \langle \xi_i(x_0), \xi_j(x_0) \rangle = \delta_{ij}, \quad (3)$$

$i, j = 1, 2$, are eigenvalues and (orientationless) normalized eigenvectors, respectively, of the Cauchy–Green (strain) tensor,

$$\mathbf{C}_{t_0}^{t_0+T}(x_0) := \mathbf{D}F_{t_0}^{t_0+T}(x_0)^\top \mathbf{D}F_{t_0}^{t_0+T}(x_0). \quad (4)$$

The tensor field $\mathbf{C}_{t_0}^{t_0+T}(x_0)$ objectively measures material deformation over the time interval $[t_0, t_0 + T]$. Limit cycles of (2) or λ -loops either grow or shrink under changes in λ , forming smooth annular regions of non-intersecting loops. The outermost member of such a band of material loops is observed physically as the boundary of a *coherent Lagrangian ring*. The λ -loops can also be interpreted as so-called null-geodesics of the indefinite tensor field $\mathbf{C}_{t_0}^{t_0+T}(x_0) - \lambda \mathbf{Id}$, which is why we also refer to them as *null-geodesic* (or *NG*) *rings*.

the flow map resulting from integrating a two-dimensional incompressible velocity field, namely, $v(x, t) = \nabla^\perp \psi(x, t)$ ($x \in \mathbb{R}^2$ and $t \in \mathbb{R}$ as stated above), where ψ denotes sea-surface height. If the pressure gradient force is exclusively due to changes in the SSH field, the latter is given by $g^{-1}f\psi(x, t)$, where g is gravity and f is the Coriolis parameter, assuming a quasigeostrophic balance.

A. Null-geodesic (NG) rings

Following Haller and Beron-Vera^{13,14} we aim to identify fluid regions enclosed by exceptional material loops that *defy the typical exponential stretching experienced by generic material loops in turbulent flows*. This is achieved by detecting loops with small annular neighborhoods exhibiting no leading-order variation in averaged material stretching.

These considerations lead to a variational problem whose solutions are loops such that any of their subsets are stretched by the same factor $\lambda > 0$ under advection by the flow from t_0 to $t_0 + T$ for some T . The time- t_0 positions of such uniformly λ -stretching material loops turn out to be limit cycles of one of the following two bidirectional vector or *line* fields:

B. Diffusion-barrier (DB) rings

Another recent approach to coherent vortices in geophysical flows has been put forward in Haller, Karrasch, and Kogelbauer¹⁶. In this case one aims at identifying fluid regions that *defy diffusive transport across their boundaries*. Note that by flow invariance, any fluid region has vanishing advective transport across its boundary. In turbulent flows, however, a generic fluid region has massive *diffusive* leakage through its boundary, which correlates with the typical exponential stretching of the latter.

A technical challenge is that the diffusive flux of a virtual diffusive tracer through a material surface over a finite time interval $[t_0, t_0 + T]$ depends on the concrete evolution of the scalar under the advection–diffusion equation. In the limit of vanishing diffusion, however, Haller, Karrasch, and Kogelbauer¹⁶ show that the diffusive flux through a material surface can be determined by the gradient of the tracer at the initial time instance and a tensor field \mathbf{T} that can be interpreted as the time average of the diffusion tensor field along a fluid trajectory. In the

case of isotropic diffusion, this reduces to the average of inverse Cauchy–Green tensors,

$$\mathbf{T}(x_0) := \frac{1}{T} \int_{t_0}^{t_0+T} (\mathbf{C}_{t_0+t}^{t_0}(x_0))^{-1} dt. \quad (5)$$

Searching for material loops with small annular neighborhoods exhibiting no leading-order variation in the vanishing-diffusivity approximation of diffusive transport leads to a variational problem whose solutions are limit cycles of (2), where now λ_i and ξ_i are, respectively, eigenvalues and eigenvectors of the time-averaged Cauchy–Green tensor

$$\bar{\mathbf{C}}_{t_0}^{t_0+T}(x_0) := \frac{1}{T} \int_{t_0}^{t_0+T} \mathbf{C}_{t_0+t}^{t_0}(x_0) dt. \quad (6)$$

This simple tensor structure assumes isotropic diffusion and an incompressible fluid flow. We refer to vortices obtained by this methodology as *diffusion-barrier* (or *DB*) *rings*. Due to the mathematical similarity to the geodesic ring approach, we may use the same computational method as for NG rings, simply by replacing $\mathbf{C}_{t_0}^{t_0+T}$ by $\bar{\mathbf{C}}_{t_0}^{t_0+T}$.

C. Rotationally-coherent (RC) rings

In our analysis, we also employ a third methodology, which was developed by Haller *et al.*¹⁵. It puts less emphasis on specific properties of the boundary (like stretching or diffusive flux) of coherent vortices, but highlights that coherent vortices are often associated with *concentrated regions of high vorticity*. Defining vortices in terms of vorticity has a long tradition,^{27,38} but in unsteady fluid flows it comes with a number of drawbacks, one of which is the lack of objectivity.¹⁰ In Haller *et al.*¹⁵, the authors overcome these challenges by showing that the *Lagrangian averaged vorticity deviation* (or *LAVD*) field

$$\text{LAVD}_{t_0}^{t_0+T}(x_0) := \int_{t_0}^{t_0+T} |\omega(F_{t_0}^t(x_0), t) - \bar{\omega}(t)| dt, \quad (7)$$

is an objective scalar field. Here, $\omega(x, t)$ is the vorticity of the fluid velocity at position x and time t , and $\bar{\omega}(t)$ is the vorticity at time t averaged over the tracked fluid bulk. In this framework, vortex centers are identified as maxima of the LAVD field, and vortex boundaries as outermost convex LAVD-level curves surrounding LAVD maxima. Because loops are composed of fluid elements that complete the same total material rotation relative to the mean material rotation of the whole fluid mass, we will refer to the vortices as *rotationally-coherent* (or *RC*) *rings*. In practice, the convexity requirement is relaxed, using a “tolerable” convexity deficiency.¹⁵ In contrast to the two previously described methods, the LAVD approach therefore does not address vortex boundaries directly (say, via a variational approach), but deduces them as level-set features of the objective LAVD field.

III. GENESIS AND APOCALYPSE

Our main goal is to study genesis, evolution, and apocalypse of LCRs from an objective, Lagrangian point of view. Since there is no generally agreed definition of the concept of a coherent vortex, we need to employ several proposed methods to rule out the possibility that the results are biased by the specific choice of method.

To determine the “birth” or the “decease” of a coherent Lagrangian vortex in a robust fashion, we need to eliminate a couple of potentially biasing issues. First, as stated above, we include several Lagrangian methodologies in our study. Second, we want to avoid potential sensitivities due to implementation details (such as algorithm or parameter choices). Recall that Lagrangian approaches choose not only an initial time instance t_0 , but also a flow horizon T . A naive approach to the determination of the decease of a coherent vortex would be to simply take the maximum of $t_0 + T$ for which a Lagrangian method detects a coherent vortex, where t_0 and T are taken from a range of reasonable values. While this approach yields a definite answer, it may be totally inconsistent with other computations run for different choices of t_0 and T . For instance, if a Lagrangian computation detects a coherent vortex over the time interval $[t_0, t_0 + T]$, it should also detect a vortex over the time interval $[t_0 + \delta t, (t_0 + \delta t) + (T - \delta t)] = [t_0 + \delta t, t_0 + T]$ for small $|\delta t|$, if $t_0 + T$ was really the date of breakdown.

In order to make our predictions statistically more robust and prove internal consistency, we employ the following approach. First, we run Lagrangian simulations on a temporal double grid as follows. We roll the initial time instance t_0 over a time window roughly covering the time interval of vortex existence, which we seek to determine. For each t_0 , we progress T in 30-day steps as long as the Lagrangian method successfully detects a coherent vortex. Thus, we obtain for each t_0 a *life expectancy* $T_{\max}(t_0)$, which is the maximum T for which a Lagrangian simulation starting at t_0 successfully detected a coherent vortex.

Ideally, we would like to see the following $T_{\max}(t_0)$ pattern. Assume a coherent Lagrangian vortex breaks down on day 200, counted from day 0. Then for $t_0 = 0$ the longest successful vortex detection should yield a $T_{\max}(0) = 180$ d. Similarly, for $t_0 = 5, 10, 15, 20$ we should get a $T_{\max} = 180$ d. From $t_0 = 25$ on, however, we should start seeing T_{\max} dropping down to 150 days, because for $T = 180$ days, the Lagrangian flow horizon reaches beyond the vortex breakdown. As a consequence, we would like to see a wedge-shaped $T_{\max}(t_0)$ distribution, which would indicate that all Lagrangian coherence assessments predict the breakdown consistently, though slightly smeared out regarding the exact date. If encountered, such a consistent prediction of breakdown would arguably remove the possibility of degenerate results. To summarize, in an ideal case, a Lagrangian simulation of the lifespan of a coherent vortex would therefore start with a large T_{\max} -value, which consistently decreases as

t_0 progresses forward in time.

It turns out that in many cases such wedge-shaped $T_{\max}(t_0)$ -patterns can be indeed observed, sometimes with astonishing clarity, given the finitely resolved velocity fields and the complexity of the Lagrangian calculation and vortex detection algorithms.

IV. DATA AND NUMERICAL IMPLEMENTATION

The SSH field from which the flow is derived is given daily on a 0.25° -resolution longitude–latitude grid. This represents an absolute dynamic topography, i.e., the sum of a (steady) mean dynamic topography and the (transient) altimetric SSH anomaly. The mean dynamic topography is constructed from satellite altimetry data, in-situ measurements, and a geoid model.³⁰ The SSH anomaly is referenced to a 20-yr (1993–2012) mean, obtained from the combined processing of data collected by altimeters on the constellation of available satellites.²²

Computationally, we detect NG and DB rings from the altimetry-derived flow by the method devised in Karrasch, Huhn, and Haller¹⁹ and recently extended for large-scale computations in Karrasch and Schilling,²⁰ as implemented in the package `CoherentStructures.jl`. It is written in the modern programming language `Julia`, and is freely available from <https://github.com/CoherentStructures/CoherentStructures.jl>. In turn, RC ring detection, computationally much more straightforward, was implemented in `MATLAB`[®] as described in Beron-Vera *et al.*² (a software tool, not employed here, is freely distributed from <https://github.com/LCSETH/Lagrangian-Averaged-Vorticity-Deviation-LAVD>). The spacing of the grid of initial trajectory positions in all cases is set to 0.1 km as in earlier Lagrangian coherence analyses involving altimetry data.^{3,4,28} Trajectory integration is carried out using adaptive time-stepping schemes and involves cubic interpolation of the velocity field data. NG and DB rings are sought with stretching parameter (λ) ranging over the interval $\lambda \in [1 \pm 0.5]$. Recall that $\lambda = 1$ NG-vortices reassume their arc length at $t_0 + T$.¹³ When the flow is incompressible (as is the case of the altimetry-derived flow) such $\lambda = 1$ vortices stand out as the most coherent of all as their boundaries resist stretching while preserving the area they enclose. Following Haller *et al.*¹⁵ the convexity deficiency is set to 10^{-3} for the RC ring extractions.

As our interest is in LCRs, we concentrate on the time intervals on which these were identified by Horizon Marine, Inc. as part of the `EddyWatch`[®] program. This program identifies LCRs as regions instantaneously filled with altimetric SSH streamlines.²³ The `EddyWatch`[®] program has been naming LCRs and reporting their birth and decease dates since 1984. Our analysis is restricted to the period 2001–2013, long enough to robustly test theoretical expectations and for the results to be useful in applications such as ocean circulation model validation.

Alternative assessments of the genesis and apocalypse of LCRs are obtained from the `AVISO+` Mesoscale Eddy Trajectory Atlas Product, which is also computed from the Eulerian footprints left by the eddies on the global altimetric SSH field.⁵

V. RESULTS

We begin by testing our expectation that Lagrangian life expectancy (T_{\max}) should decrease with increasing screening time (t_0), exhibiting a wedge shape. We do this by focusing on LCR *Kraken*, so named by `EddyWatch`[®] and recently subjected to a Lagrangian coherence study.³ In that study the authors characterized *Kraken* as an NG ring using altimetry data. Furthermore, they presented support for their characterization by analyzing independent data, namely, satellite-derived color (Chl concentration) and trajectories from satellite-tracked drifting buoys. This rules out the possibility that LCR *Kraken* is an artifact of the satellite altimetric dataset, thereby constituting a solid benchmark for testing our expectation. The authors of the aforementioned study estimated a Lagrangian lifetime for *Kraken* of about 200 d, but framing the genesis and apocalypse of the ring with precision was beyond the scope of their work.

The top panel of Fig. 1 shows $T_{\max}(t_0)$ for *Kraken* based on NG (red), DB (solid black), and RC (dashed black) coherence assessments. First note that the NG and DB assessments are largely consistent, producing a wide-base $T_{\max}(t_0)$ wedge with height decreasing with increasing t_0 in addition to a short, less well-defined wedge prior to it. This becomes very evident when compared to the RC assessment, which produces intermittent wedge-like $T_{\max}(t_0)$ on various short t_0 -intervals. We have observed that this intermittency is typical, rather than exceptional, for the RC assessment. Thus we consider NG coherent Lagrangian vortex detection, which in general produces nearly identical results as DB vortex detection, in the genesis and apocalypse assessments that follow.

Indicated in the top panel of Fig. 1 (with a vertical dashed line) is our estimate of the birth date of LCR *Kraken*, $t_0 = 18/\text{May}/2013$, and three estimates of its decease date, to wit, $t_0 = 12/\text{Jan}/2014$, $21/\text{Feb}/2014$, and $21/\text{Apr}/2014$. The birth date corresponds to the t_0 marking the leftmost end of the $T_{\max}(t_0)$ wedge with the longest base (highlighted). Our first decease date estimate (d1) is given by the birth date plus its life expectancy, set by the height of the wedge or $12/\text{Jan}/2014 - 18/\text{May}/2013 = 239$ d. The second decease date estimate (d2) is given by the t_0 marking the rightmost end of the wedge, which is 40-d longer than its life expectancy. Our third decease date estimate (d3) is given by the second decease date estimate plus the height of the wedge at its rightmost end, namely, $21/\text{Apr}/2014 - 21/\text{Feb}/2014 = 59$ d.

The bottom panel of the Fig. 1 shows, in orange, LCR *Kraken* on its estimated birth date (b), and its advected

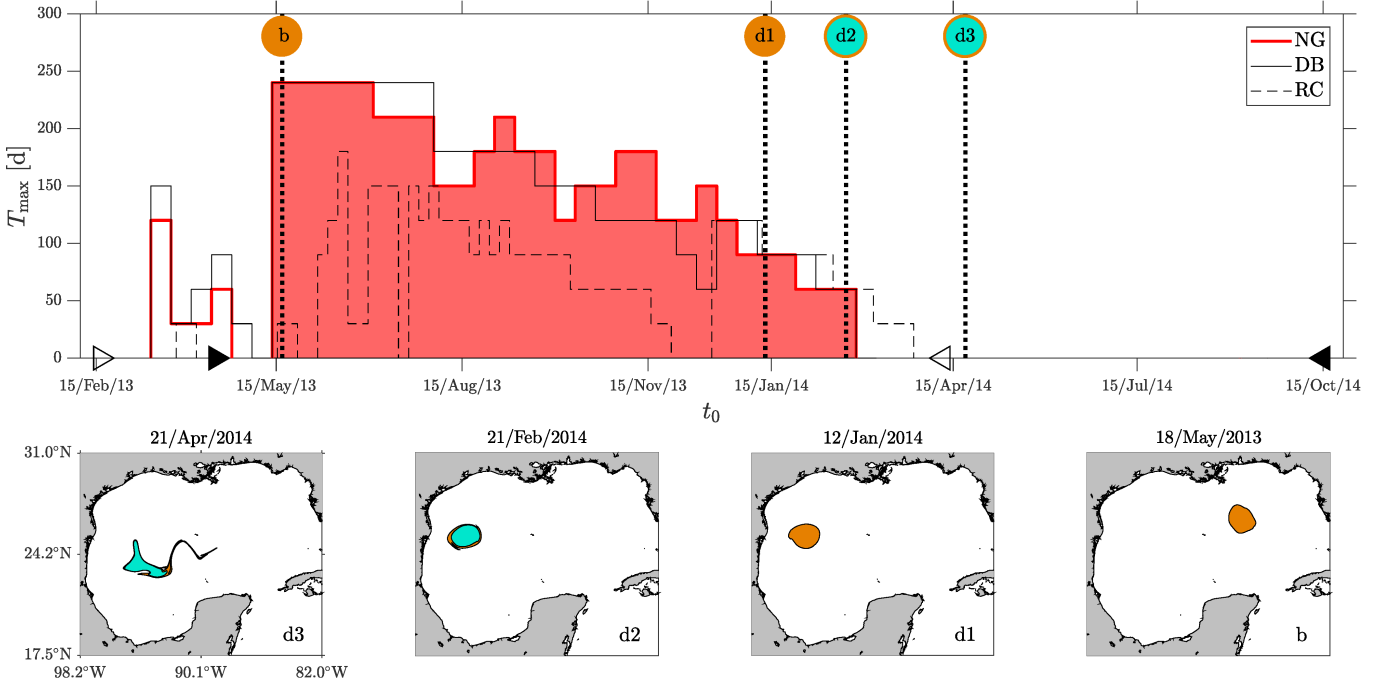


FIG. 1. (top panel) For Gulf of Mexico's Loop Current ring (LCR) *Kraken*, life expectancy as a function of screening time according null-geodesic (NG), diffusion-barrier (DB), and rotationally-coherent (RC) Lagrangian vortex assessments. Indicated are the birth date of the ring (b), and three decease date estimates (d1, d2, and d3); cf. text for details. Birth and decease dates according to EddyWatch[®] and AVISO+ Eulerian vortex assessments are indicated with open and filled triangles, respectively. (bottom panel) Based on the NG assessment, LCR *Kraken* on birth date and the three decease date estimates.

image under the altimetry-derived flow on the first (d1), second (d2), and third (d3) decease date estimates. Overlaid on the later on the second and third decease date estimated are (shown in cyan) the NG vortex extracted on the second decease date estimate and its advected image on the third decease date estimate. Note that on the first and second decease date estimates *Kraken* does not show any noticeable signs of outward filamentation. On the third decease date estimate most of the original fluid mass enclosed by the ring boundary exhibits a coherent aspect. Evidently, the first and second decease date estimates are too conservative, so it is reasonable to take the third one as the most meaningful decease date estimate of the three. We will refer to it as *the* decease date.

Indicated by open and filled triangles in the abscissa of the $T_{\max}(t_0)$ plot in the top panel of the Fig. 1 are the Eulerian assessment of birth and decease dates of *Kraken* by EddyWatch[®], and AVISO+, respectively. EddyWatch[®] overestimates the decease date by about 180 d, while AVISO+, underestimates it somewhat, by 19 d. To evaluate the performance of Eulerian vortex detection in assessing the birth date of *Kraken* an additional analysis is needed.

The results from such an analysis are presented in Fig. 2, which shows the same as in Fig. 2 but as obtained from applying all the Lagrangian vortex detection methods *backward* in time, i.e., with $T < 0$, around the *Kraken's* decease date. The top panel of the fig-

ure shows (now) $|T_{\max}|$ as a function of screening time t_0 . Note that the NG and DB coherence assessments produce single wide-base $|T_{\max}|(t_0)$ wedges with height decreasing with decreasing t_0 , nearly indistinguishable from one another. As in the forward-time analysis, the RC assessment shows intermittent wedge-like $|T_{\max}|(t_0)$ on various short t_0 -intervals, suggesting a much shorter life expectancy than observed in reality. Thus we turn our attention to the NG (or DB) assessment. This produces a backward-time birth date estimate on $t_0 = 02/\text{Apr}/2014$, and three backward-time decease date estimates on $06/\text{Apr}/2013$, $08/\text{Apr}/2013$, and $10/\text{Mar}/2013$. In forward time, $02/\text{Apr}/2014$ represents a decease date estimate, which is only 19-d earlier than the decease date obtained above from forward-time computation. The largest discrepancy between forward- and backward-time assessments are seen for the birth date. Following the forward-time computation reasoning above, the backward-time computations sets it 296 d earlier, on $t_0 = 10/\text{Mar}/2013$. This lies 21 and about 30 d later and earlier than to the AVISO+ and EddyWatch[®], assessments, respectively, which are instantaneous, i.e., they do not depend on the time direction on which they are made.

The backward-time estimate of *Kraken's* decease date can be taken to represent a forward-time *conception* date estimate for the ring. This is quite evident from the inspection of the bottom panel of Fig. 2, which shows (in orange) LCR *Kraken* as extracted from backward-time

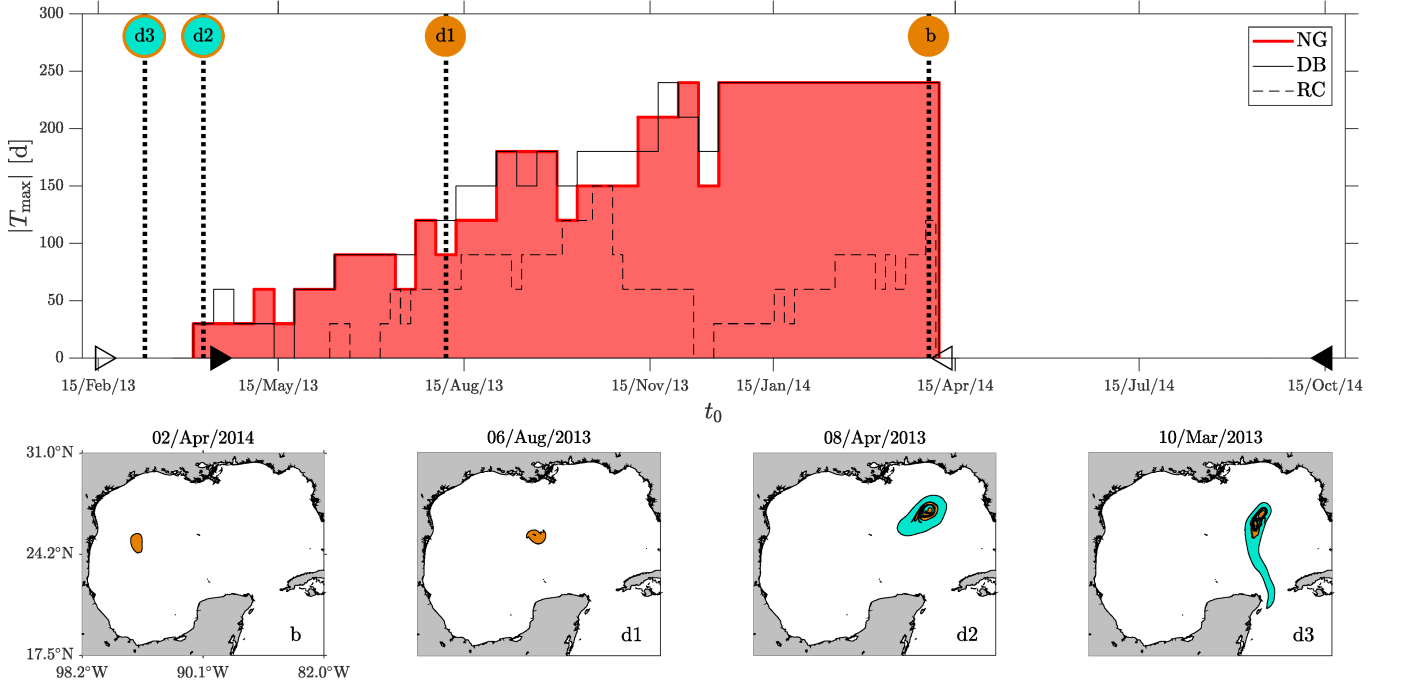


FIG. 2. As in Fig. 1, but for assessments made in backward time.

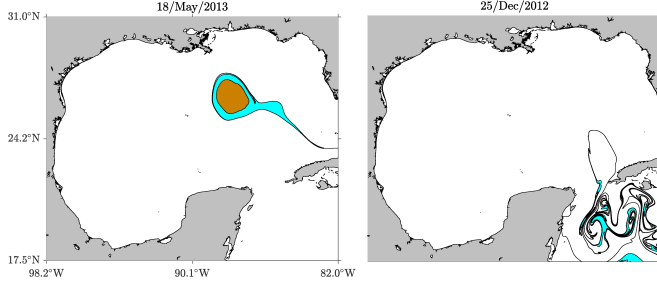


FIG. 3. (left panel) LCR *Kraken* on birth date overlaid in orange on the forward-advected image of the ring extracted from backward-time computation on 08/Apr/2013 (third backward-time decease estimate). (right panel) Backward-advected image of the fluid region indicated in cyan in the left panel.

computation on the backward-time birth date estimate, and images thereof under the backward-time flow on the three backward-time decease date estimates. On the last two decease date estimates, these are shown overlaid on the ring extracted from backward-time computation on the second backward-time decease date estimate and its backward-advected image on the third backward-time decease date estimate, which represents, as noted above, a conception date for *Kraken*.

Indeed, the fluid region indicated in cyan contains at all times the fluid region indicated in orange. Thus the orange fluid is composed of the same fluid as the cyan fluid. Furthermore, the cyan fluid, which can be traced back into the Caribbean Sea, ends up forming the fluid that forms *Kraken* on its (forward-time) birth date. This

is illustrated in left panel of Fig. 3, which shows *Kraken* (in orange) as obtained from forward-time computation on its birth date overlaid on the forward-advected image of the cyan fluid. In the right panel we show a backward-advected image of the cyan fluid that reveals its origin in the Caribbean Sea. The supplementary material includes an animation (Mov. 1) illustrating the full life cycle of LCR *Kraken*.

We note that the need of introducing the conception date estimate could have been anticipated from the inspection of the forward-time assessment. Note the short wedge-like $T(t_0)$ before the long-base wedge in Fig. 1 employed in assessing genesis and apocalypse. In a way the presence of that short wedge-like $T(t_0)$ was already insinuating that coherence was building sometime before the ring was declared born. Similar disconnected wedge-like $T(t_0)$ patterns may be observed past the main wedge, as can be seen in Fig. 4, which shows the same as Fig. 1 but for LCR *Yankee*. These wedge-like patterns, however, are not signs of the ring’s “resurrection,” but actually correspond to vortex structures in general unrelated or only partly related to the ring in question.

We illustrate the above in Fig. 5. Note the appearance of two short wedge-like patterns past the main $T(t_0)$ wedge. Let us concentrate attention on the earliest of the two short wedges. We infer a forward-time birth date is 30/Jun/2007, and two forward-time decease dates on 18/Sep/2017 and 17/Oct/2017. The bottom panels of the figure show how these characterize the life cycle of a vortex, newly formed and composed only in part of LCR *Yankee*’s fluid. This is evident by comparing the position of the vortex on birth date and first decease date esti-

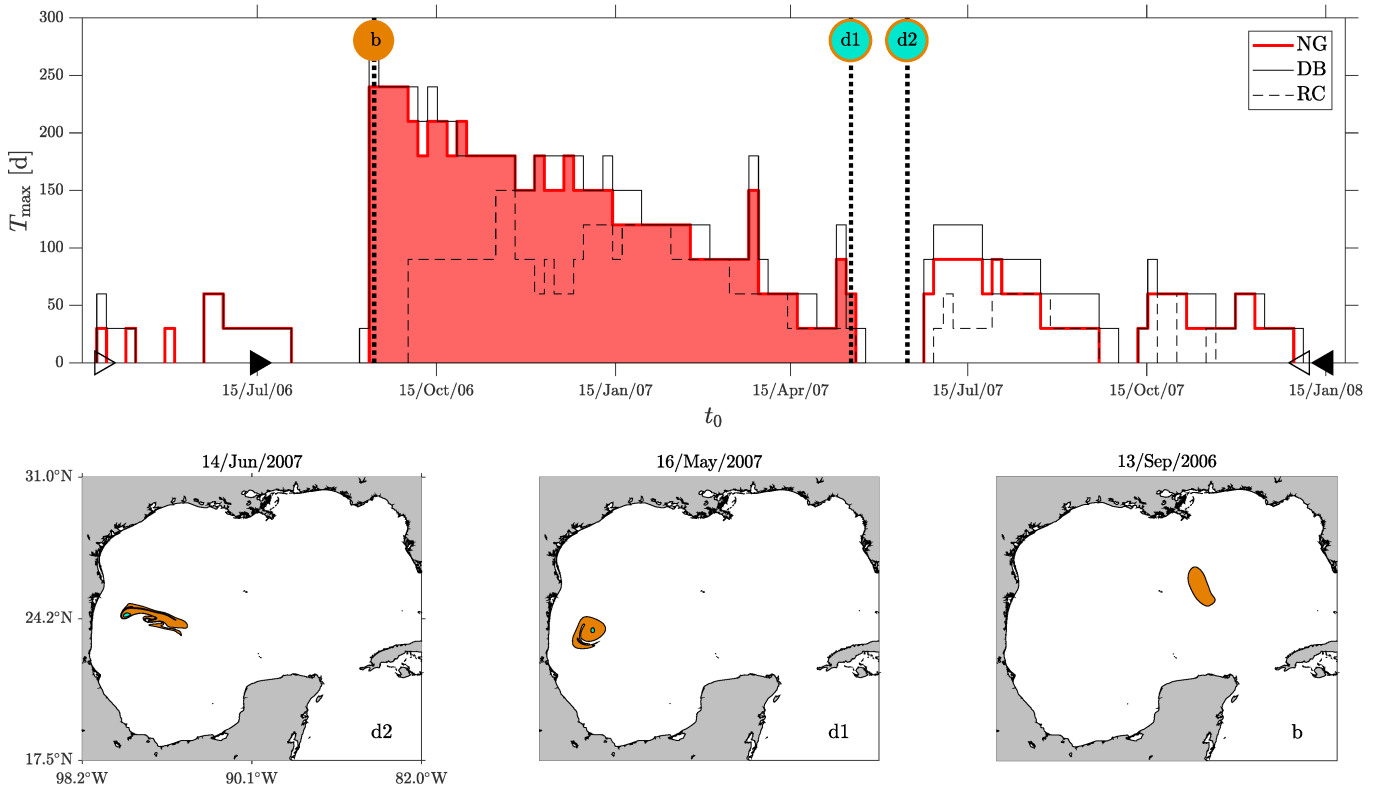


FIG. 4. As in Fig. 1, but for LCR *Yankee*.

mates and their forward-advected images with those of *Yankee* as revealed on 13/Sep/2006. The EddyWatch[®] and AVISO+ nonobjective Eulerian vortex assessments fail to frame this, largely overestimating the decease date of *Yankee*.

We compile in Table I the objective Lagrangian estimates of conception, birth, and decease dates for all LCRs during the altimetry era. An entry of table left blank means that the ring could not be classified as coherent. The objective estimates are compared with nonobjective Eulerian estimates by EddyWatch[®] and AVISO+, with the former only providing the month of the year when birth and decease take place. Note the tendency of the Eulerian assessments to overestimate the birth and decease dates of the rings. Indeed, the Eulerian assessments cannot distinguish between conception and birth. They typically keep track of vortex-like structures past the decease date of the rings, which, present around that date, are not formed by the fluid mass contained by the rings. Moreover, the Eulerian assessments classify as coherent, and even name, rings that turn out not to be so. The supplementary material includes two animations supporting these conclusions for features classified as LCRs *Quick* (Mov. 2) and *Sargassum* (Mov. 3) by the EddyWatch[®] and AVISO+ nonobjective Eulerian assessments.

We conclude by highlighting the disparities between the objective Lagrangian and nonobjective Eulerian assessments of the genesis and apocalypse of LCR rings

in Fig. 6. The figure presents, as a function of time over 2001–2011, the difference (in d) between NG and E (dots), and NG and A (circles) assessments of birth (left) and decease (right) dates. The differences can be quite large (up to 1 yr!) with Eulerian assessments, which in general underestimate the birth dates of the rings and overestimate their decease dates.

VI. CONCLUSIONS

We have carried out an objective (i.e., observer-independent) Lagrangian assessment of the life cycle of the Loop Current rings (LCRs) in Gulf of Mexico detected from satellite altimetry. Three objective methods of coherent Lagrangian vortex detection were considered here. These reveal material vortices with boundaries that defy stretching or diffusion, and whose elements rotate evenly. A modest technology advance was performed which enabled framing vortex genesis and apocalypse with robustness and precision. We found that the stretching- and diffusion-defying assessments produce consistent results. These in general showed large discrepancies with Eulerian assessments which identify vortices with regions instantaneously filled with streamlines of the SSH field. The Eulerian assessments were found incapable to distinguish conception from birth of the rings. They also tended to track past their decease dates vortex-like features unrelated to the rings in question. The even-

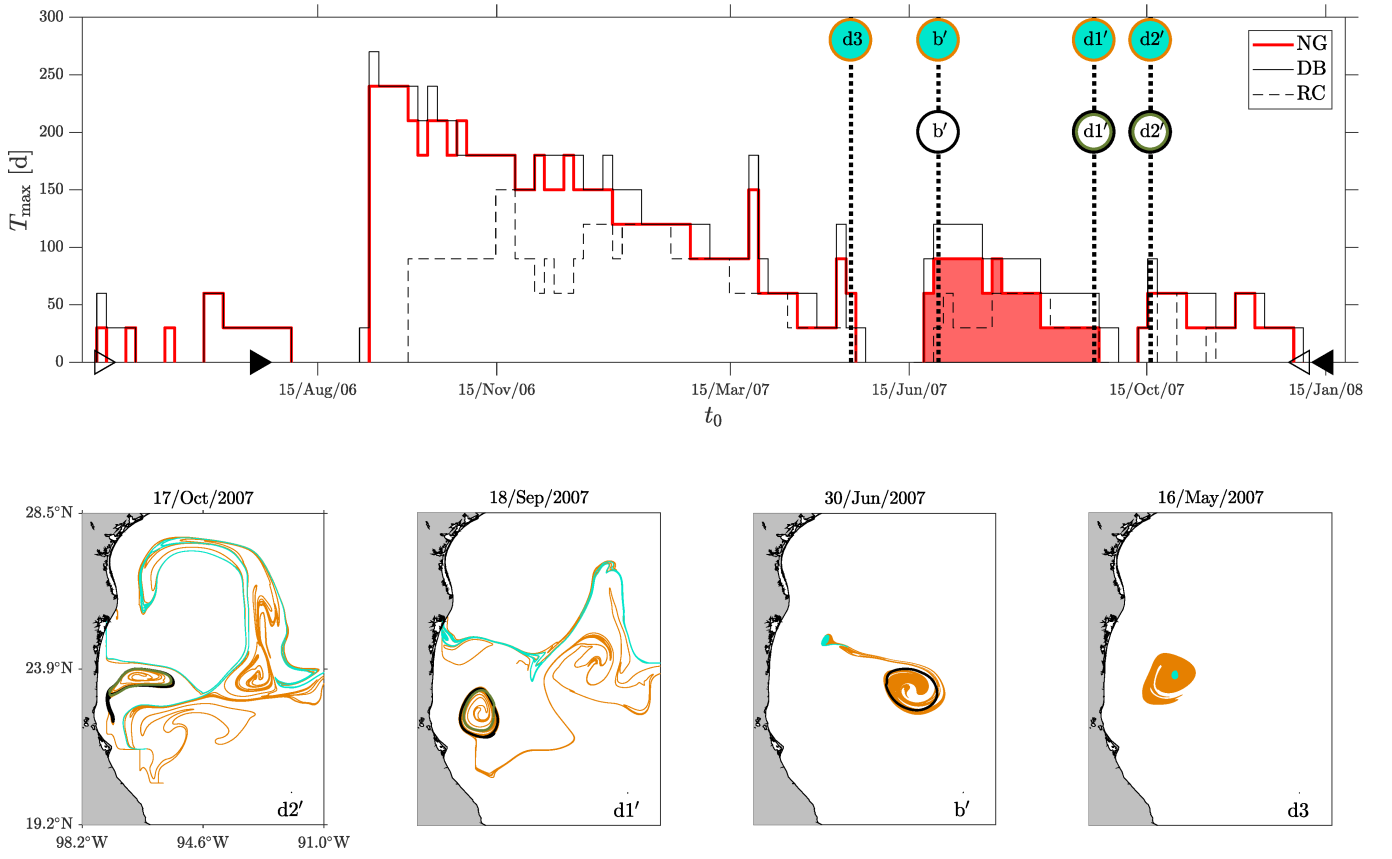


FIG. 5. As in Fig. 4, with a focus on the highlighted piece of the $T_{\max}(t_0)$ plot.

Ring	Conception date	Birth date			Decease date		
		Objective	EddyWatch [®]	AVIS0+	Objective	EddyWatch [®]	AVIS0+
<i>Nansen</i>	27/02/01	13/03/01	04/01	18/03/00	31/07/01	12/01	04/01/02
<i>Odesa</i>	02/07/01	31/07/01	09/01	23/03/01	09/10/01	12/01	05/11/01
<i>Pelagic</i>			12/01	07/09/01		05/02	17/02/02
<i>Quick</i>			03/02	19/02/02		04/03	05/05/03
<i>Sargasum</i>			05/03	30/03/02		12/03	16/01/04
<i>Titanic</i>	10/11/03	09/12/03	10/03	01/08/03	21/06/04	10/04	13/11/04
<i>Ulises</i>	22/11/04	11/12/04	05/04	07/12/03	15/05/05	09/05	07/10/05
<i>Extreeme</i>			03/06	13/01/06		09/06	13/11/06
<i>Yankee</i>	04/09/06	13/09/06	07/06	26/04/06	31/05/07	01/08	03/01/08
<i>Zorro</i>	10/03/07	24/03/07	04/07	26/08/06	16/08/07	08/07	17/08/07
<i>Albert</i>	02/11/07	01/12/07	11/07	21/03/07	05/03/08	05/08	23/04/08
<i>Cameron</i>	20/06/08	20/06/08	07/08	15/06/08	10/02/09	05/09	18/06/09
<i>Darwin</i>	29/01/09	02/02/09	12/08	13/02/08	25/10/09	11/09	10/11/09
<i>Ekman</i>	11/04/09	09/07/09	07/09	04/02/09	20/05/10	03/11	28/08/10
<i>Hadal</i>	22/06/11	11/07/11	08/11	23/11/10	23/12/11	03/12	26/12/11
<i>Icarus</i>	08/10/11	22/10/11	11/11	19/07/11	11/09/12	02/13	04/10/12
<i>Jumbo</i>	28/04/12	28/04/12	06/12	18/04/12	21/08/12	02/13	10/11/12
<i>Kraken</i>	10/03/13	08/04/13	04/13	17/02/13	02/04/14	10/14	10/04/14

TABLE I. Objective Lagrangian estimates of conception, birth, and decease dates of Loop Current rings in the Gulf of Mexico identified from satellite altimetry over 2001–2013 along with nonobjective Eulerian estimates of birth and decease dates.

rotation assessment, which is vorticity-based, was found to be quite unstable, suggesting life expectancies much

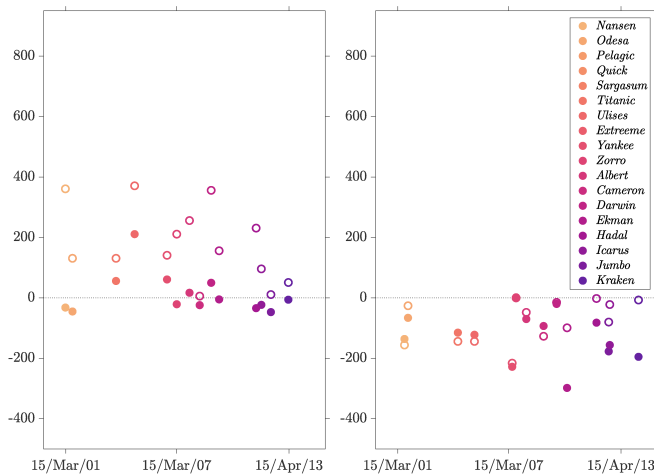


FIG. 6. As a function of time, difference (in d) between objective Lagrangian and nonobjective Eulerian estimates of birth (left panel) and death (right panel) dates. Dots (resp., circles) involve EddyWatch[®], (resp., AVISO+) assessments.

shorter than those produced by all other assessments. The inconsistency found adds to the list of known issues of LAVD-based vortex statistics,³⁵ including high sensitivity with respect to the choice of computational parameter values. Our results can find value in drawing unambiguous evaluations of material transport and should represent a solid metric for ocean circulation model benchmarking.

SUPPLEMENTARY MATERIAL

The supplementary material contains three animations. Movie 1 illustrates the complete life cycle of LCR *Kraken* as assessed objectively using NG-ring detection. Movies 2 and 3 show sequences of advected images of the features classified as LCRs *Quick* and *Sargassum*, respectively, by the EddyWatch[®] and AVISO+ nonobjective Eulerian assessments.

AUTHOR'S CONTRIBUTIONS

All authors contributed equally to this work.

ACKNOWLEDGMENTS

This work was initiated during the “Escuela interdisciplinaria de transporte en fluidos geofísicos: de los remolinos oceánicos a los agujeros negros,” Facultad de Ciencias Exactas y Naturales, Universidad de Buenos Aires, 5–16/Dec/2016. Support from Centro Latinoamericano de Formación Interdisciplinaria is sincerely appreciated. This work was supported by CONACyT–SENER (Mexico) under Grant No. 201441 (FAC, FJBV) as part

of the Consorcio de Investigación del Golfo de México (CIGoM). FAC thanks CICESE (Mexico) for allowing him to use their computer facilities throughout the CIGoM project.

AIP PUBLISHING DATA SHARING POLICY

The gridded multimission altimeter products were produced by SSALTO/DUACS and distributed by AVISO+ (<https://www.aviso.altimetry.fr/>), with support from CNES. The Mesoscale Eddy Trajectory Atlas Product was produced by SSALTO/DUACS and distributed by AVISO+ (<https://www.aviso.altimetry.fr/>) with support from CNES, in collaboration with Oregon State University with support from NASA. The EddyWatch[®] data are available from Horizon Marine, Inc.'s website at <https://www.horizonmarine.com/>.

- ¹Andrade-Canto, F., Sheinbaum, J., and Sansón, L. Z., “A Lagrangian approach to the Loop Current eddy separation,” *Nonlin. Processes Geophys.* **20**, 85–96 (2013).
- ²Beron-Vera, F. J., Hadjighasem, A., Xia, Q., Olascoaga, M. J., and Haller, G., “Coherent Lagrangian swirls among submesoscale motions,” *Proc. Natl. Acad. Sci. U.S.A.* **116**, 18251–18256 (2019).
- ³Beron-Vera, F. J., Olascoaga, M. J., Wang, Y., Triñanes, J., and Pérez-Brunius, P., “Enduring Lagrangian coherence of a Loop Current ring assessed using independent observations,” *Scientific Reports* **8**, 11275 (2018).
- ⁴Beron-Vera, F. J., Wang, Y., Olascoaga, M. J., Goni, G. J., and Haller, G., “Objective detection of oceanic eddies and the Agulhas leakage,” *J. Phys. Oceanogr.* **43**, 1426–1438 (2013).
- ⁵Chelton, D. B., Schlax, M. G., and Samelson, R. M., “Global observations of nonlinear mesoscale eddies,” *Prog. Oceanogr.* **91**, 167–216 (2011).
- ⁶Donohue, K., Watts, D., Hamilton, P., Leben, R., and Kennelly, M., “Loop current eddy formation and baroclinic instability,” *Dynamics of Atmospheres and Oceans* **76**, 195–216 (2016), the Loop Current Dynamics Experiment.
- ⁷Forristall, G. Z., Schaudt, K. J., and Cooper, C. K., “Evolution and kinematics of a Loop Current eddy in the Gulf of Mexico during 1985,” *J. Geophys. Res.* **97**, 2173–2184 (1992).
- ⁸Hadjighasem, A., Farazmand, M., Blazeviski, D., Froyland, G., and Haller, G., “A critical comparison of Lagrangian methods for coherent structure detection,” *Chaos* **27**, 053104 (2017).
- ⁹Haller, G., “An objective definition of a vortex,” *J. Fluid Mech.* **525**, 1–26 (2005).
- ¹⁰Haller, G., “Lagrangian coherent structures,” *Ann. Rev. Fluid Mech.* **47**, 137–162 (2015).
- ¹¹Haller, G., “Climate, black holes and vorticity: How on Earth are they related?” *SIAM News* **49**, 1–2 (2016).
- ¹²Haller, G. and Beron-Vera, F. J., “Geodesic theory of transport barriers in two-dimensional flows,” *Physica D* **241**, 1680–1702 (2012).
- ¹³Haller, G. and Beron-Vera, F. J., “Coherent Lagrangian vortices: The black holes of turbulence,” *J. Fluid Mech.* **731**, R4 (2013).
- ¹⁴Haller, G. and Beron-Vera, F. J., “Addendum to ‘Coherent Lagrangian vortices: The black holes of turbulence’,” *J. Fluid Mech.* **755**, R3 (2014).
- ¹⁵Haller, G., Hadjighasem, A., Farazmand, M., and Huhn, F., “Defining coherent vortices objectively from the vorticity,” *J. Fluid Mech.* **795**, 136–173 (2016).
- ¹⁶Haller, G., Karrasch, D., and Kogelbauer, F., “Material barriers to diffusive and stochastic transport,” *Proceedings of the National Academy of Sciences* **115**, 9074–9079 (2018).

- ¹⁷Haller, G., Karrasch, D., and Kogelbauer, F., “Barriers to the transport of diffusive scalars in compressible flows,” *SIAM Journal on Applied Dynamical Systems* **19**, 85–123 (2020).
- ¹⁸Kantha, L., “Empirical models of the loop current eddy detachment/separation time in the gulf of mexico,” *Journal of Waterway, Port, Coastal, and Ocean Engineering* **140**, 04014001 (2014).
- ¹⁹Karrasch, D., Huhn, F., and Haller, G., “Automated detection of coherent Lagrangian vortices in two-dimensional unsteady flows,” *Proc. Royal Soc. A* **471**, 20140639 (2014).
- ²⁰Karrasch, D. and Schilling, N., “Fast and robust computation of coherent lagrangian vortices on very large two-dimensional domains,” *The SMAI journal of computational mathematics* **6**, 101–124 (2020).
- ²¹Kuznetsov, L., Toner, M., Kirwan, A. D., Jones, C. K. R. T., Kantha, L. H., and Choi, J., “The Loop Current and adjacent rings delineated by Lagrangian analysis of the near-surface flow,” *J. Mar. Res.* **60**, 405–429 (2002).
- ²²Le Traon, P. Y., Nadal, F., and Ducet, N., “An improved mapping method of multisatellite altimeter data,” *J. Atmos. Oceanic Technol.* **15**, 522–534 (1998).
- ²³Leben, R. R., “Altimeter-derived loop current metrics,” in *Circulation in the Gulf of Mexico: Observations and Models*, edited by W. Sturges and A. Lugo-Fernandez (American Geophysical Union, 2005) pp. 181–201.
- ²⁴Lewis, J. K. and Kirwan, A. D., “Genesis of a Gulf of Mexico ring as determined from kinematic analyses,” *J. Geophys. Res.* **92**, 11727–11740 (1987).
- ²⁵Lipphardt, B. L., Poje, A. C., Kirwan, A. D., Kantha, L., and Zweng, W., “Death of three Loop Current rings,” *J. Marine Res.* **66**, 25–60 (2008).
- ²⁶Lugt, H. J., “The dilemma of defining a vortex,” in *Recent Developments in Theoretical and Experimental Fluid Mechanics*, edited by U. Muller, K. G. Riesner, and B. Schmidt (Springer-Verlag, 1979) pp. 309–321.
- ²⁷Okubo, A., “Horizontal dispersion of floatable particles in the vicinity of velocity singularity such as convergences,” *Deep-Sea Res. Oceanogr. Abstr.* **12**, 445–454 (1970).
- ²⁸Olascoaga, M. J., Beron-Vera, F. J., Haller, G., Trinanès, J., Iskandarani, M., Coelho, E. F., Haus, B., H. S. Huntley, G. J., D. Kirwan, Jr., A., Lipphardt, Jr., B. L., Özgökmen, T., Reniers, A. J. H. M., and Valle-Levinson, A., “Drifter motion in the Gulf of Mexico constrained by altimetric Lagrangian Coherent Structures,” *Geophys. Res. Lett.* **40**, 6171–6175 (2013).
- ²⁹Peacock, T., Froyland, G., and Haller, G., “Introduction to focus issue: Objective detection of coherent structures,” *Chaos* **25**, 087201 (2015).
- ³⁰Rio, M.-H. and Hernandez, F., “A mean dynamic topography computed over the world ocean from altimetry, in situ measurements and a geoid model,” *J. Geophys. Res.* **109**, C12032 (2004).
- ³¹Serra, M. and Haller, G., “Objective Eulerian coherent structures,” *Chaos* **26**, 053110 (2016).
- ³²Shay, L. K., Goni, G. J., and Black, P. G., “Effects of a warm oceanic feature on hurricane opal,” *Mon. Weather Rev.* **128**, 1366–1383 (2000).
- ³³Sturges, W. and Leben, R., “Frequency of ring separation from the Loop Current in the Gulf of Mexico: A revised estimate,” *J. Phys. Oceanogr.* **30**, 1814–1819 (2000).
- ³⁴Sturges, W. and Lugo-Fernandez, A., “Circulation in the gulf of mexico: Observations and models,” Washington DC American Geophysical Union Geophysical Monograph Series **161** (2005).
- ³⁵Tarshish, N., Abernathey, R., Zhang, C., Dufour, C. O., Frenger, I., and Griffies, S. M., “Identifying lagrangian coherent vortices in a mesoscale ocean model,” *Ocean Modelling* **130**, 15 – 28 (2018).
- ³⁶Wang, Y., Olascoaga, M. J., and Beron-Vera, F. J., “Coherent water transport across the South Atlantic,” *Geophys. Res. Lett.* **42**, 4072–4079 (2015).
- ³⁷Wang, Y., Olascoaga, M. J., and Beron-Vera, F. J., “The life cycle of a coherent Lagrangian Agulhas ring,” *J. Geophys. Res.* **121**, 3944–3954 (2016).
- ³⁸Weiss, J., “The dynamics of enstrophy transfer in two-dimensional hydrodynamics,” *Physica D* **48**, 273–294 (1991).